STM JOURNALS

Journal of
Materials & Metallurgical Engineering

https://journals.stmjournals.com/jomme

ISSN: 2231-3818 (Online)
ISSN: 2321-4236 (Print)
Volume 15, Issue 2, 2025
May–August
DOI (Journal): 10.37591/JoMME

Review JoMME

Heat Transfer by Arc Welding for a Similar Material Joint

Md. Riazuddin[1], Santosh Kumar Panda[2,*], Achyutananda Parida[3], Gedela Vasudev[4]

Abstract

Electric arc welding (EAW) is a traditional fabrication process used in wider domestic, commercial and industrial application. Welding is a joining of two materials with the application of heat at the molecular level with the application of heat and pressure. Many materials used for welding application for different joining process. Maraging steel is special steel used for production of different air-craft components. Maraging material is used for heavy tools, producing strength, toughness, weld ability, and machine ability is good for any components. The investigation of heat transfer during the welding for a maraging steel surface provides a new topic for the research. The ranges of input parameters are voltage (35 to 55 V), current (70 to 90 V) and electrode diameter (5 to 20 mm). The study also predicts the effect of mode of heat transfer for the welding environment. The mode of heat transfer considered for the studies are convection on the variation of heat transfer coefficient and mixed effects of convection – radiation. The heat transfer coefficient is varies 0 to 100 W/m^2 K. The present study considered the considerations such as voltage, current and electrode diameter to determine the weld energy produced through the welding. The study will also find the temperature profile, heat dissipation rate of the welding zone and work piece. The study will contribute to knowing the characteristics and phenomenon of electric arc welding for heat transfer phenomenon. The present work also helps to design and joining of the components for industrial and air craft components.

Keywords: Welding, electric arc welding, heat flux, weld zone, heat transfer, maraging steel

INTRODUCTION

Day-to-day, new materials are developed to improve the component's performance and durability. Maraging steel composites are the newest welding materials, having a composition of iron, carbon, nickel, cobalt, molybdenum, and titanium. The material is used in manufacturing aircraft components and heavy tools, offering good strength, toughness, weldability, and machinability. The material provides good dimensional stability due to excessive heat control, which manages the micrograin structure. Welding is a fabrication process that changes the structure of the material with molecular restructuring through the application of heat. Electric arc welding is used in every aspect of daily life as well as industrial applications. The study of welding from different perspectives is easily understood through graphical representations and simulations based on computations derived from practical conditions. The intend of the work is to conduct a numerical analysis to determine the overall welding characteristics of maraging steel before carrying out expensive experimental analysis. The characteristics of welding are presented in a numerical simulation using advanced commercial tools to study the heat transfer phenomenon in maraging steel.

***Author for Correspondence**
Santosh Kumar Panda
E-mail: santumech83@gmail.com

[1-4]Assistant Professor, Department of Mechanical Engineering, National Institute of Science and Technology (NIST) University, Berhampur, Odisha, India

Received Date: February 17, 2025
Accepted Date: March 08, 2025
Published Date: March 11, 2025

Citation: Md. Riazuddin, Santosh Kumar Panda, Achyutananda Parida, Gedela Vasudev. Heat Transfer by Arc Welding for a Similar Material Joint. Journal of Materials & Metallurgical Engineering. 2025; 15(2): 1–13p.

The various arc welding parameters includes welding current, arc voltage, welding speed, heat, and polarity. Welding Current is used during welding. It directly affects the heat input, depth of penetration, etc. Voltage is controls the arc length. Welding Speed is the speed at which the electrode travels along the welding joint. More speed causes insufficient heat input leading to incomplete weld joint. Lower speed causes more heat input to the welding joint leading to burnouts. Polarity: It decides the direction of current flow between the electrode and work piece which in turn decides the heat input at the work piece. These arc welding parameters directly affects the weld quality and welding efficiency. Optimization of these parameters reduces welding defects and produces sound quality weld which has important applications in various industries like automotives, construction, and aerospace. Durable welding joints are crucial for joining chassis parts in automobiles.

Numerical study of welding of dissimilar material with its properties are reported (Hejripour et al., 2019; Liang and Luo, 2017; Wei et al., 2015).[14, 23, 38] Heat transfer analysis of friction stir welding for dissimilar materials of Al and Cu alloys are carried out by ANSYS (Kumar et al., 2025). [19] Temperature distribution by friction stirs welding of the magnesium-based alloy AZ31B-H24 (Sati et al., 2018). [28] Temperature and stress distribution of plasma arc welding for titanium sheet (Hossain et al., 2024),[15] thermal modeling of TIG welding using ANSYS for 304 stainless steel (Prabakaran et al., 2022),[34] density of heat transfer in electron beam welding of Ti and Al alloy (Murygin et al., 2021). [24] Stress analysis of arc welding by 3D numerical analysis was conducted (Campagnolo et al., 2021; Arunkumar et al., 2019),[2, 6] submerged arc welding of Ramor 500 armor steels (Taskaya et al., 2019). [30]

The numerical simulations of fusion-based butt welding on identical geometrical profile are considered (Patterson et al., 2021; Zhang et al., 2020; Xu et al., 2019; Chukkan et al., 2015; Tsirkas et al., 2003). [17, 26, 35, 39, 40] Thermo-mechanical welding of a double U-shaped joint of alloy steel to compute stress and heat distribution to predict the temperature distribution. Arc welding, submerged arc welding process (Chen et al., 2012), [7] thermo-mechanical and residual stress distribution (Sattari-Far et al., 2009) [33] of mild steel evaluated for a butt joint. Circumferential surface of a cylindrical weld by TIG and temperature and heat transfer analysis (Arora et al., 2022), [1] heat transfer analysis of bimetallic rings by electron beam welding (Kuraskin et al., 2021), [20] applied circumferential heat flux to weld structural steel plates to determine temperature and stress distribution of the welding joint were carried out (Vemanaboina et al., 2014). [36] Unsteady thermal behaviour of a T-joint of stainless steel was used to evaluate and perform temperature distribution.

A number of heat sources and geometries are considered for heat transfer analysis for Gas Tungsten Arc Welding (GTAW) and Gas Metal Arc Welding (GMAW) (Farias et al., 2022),[11] GTAW applied to SS316L (Reddy et al., 2023), [27] and GMAW (Schnick et al., 2011).[29] A Gaussian heat source was implemented to find temperature and stress analysis of a welding process on a fused silica substrate (Tan et al., 2019).[16] The temperature profile of twin-arc submerged arc welding for a welding surface was determined (He et al., 2011). [13] The complexity of heat transfer involves different modes such as conduction, convection, and radiation in welding, as described (Lancaster, 1986). [21] The dependent parameters of the material, geometrical shape and size of the workpieces, power density and welding speed, are presented (Ebrahimi et al., 2023; Chludzinski et al., 2021; Ayoola et al., 2017; Baruah and Bag, 2017; Collins E., E., Joseph I. A., 2017). [4,5,8,9, 10]

A 3D moving coordinate FSW technique was used to predict the heat transfer and temperature distribution for tool AA6082 (Verma et al., 2017),[37] AA7075 and AA2024 (Padmanaban et al., 2014), [25] AA7020-T53 (Aval et al., 2010), [3] and AA6061 tool (Song et al., 2003). [32] (Jain et al., 2017) [18] conducted the welding under various thermal conditions for tool AA2024 and found the deformation effects on rotational and welding speed. Based on the above literature study, a heat transfer analysis of maraging steel through electric arc welding, considering the variation of the supply electrode diameter, current, and voltage, will be predicted. The study also considers the effects of different heat

transfer modes during the welding process. This study will help in analyzing the welding of the above-mentioned material.

NUMERICAL SIMULATION

The numerical study conducted by modeling a T-section of the required size as shown in Figure 1. The mesh geometry of the T-section model is presented in the Figure 2.

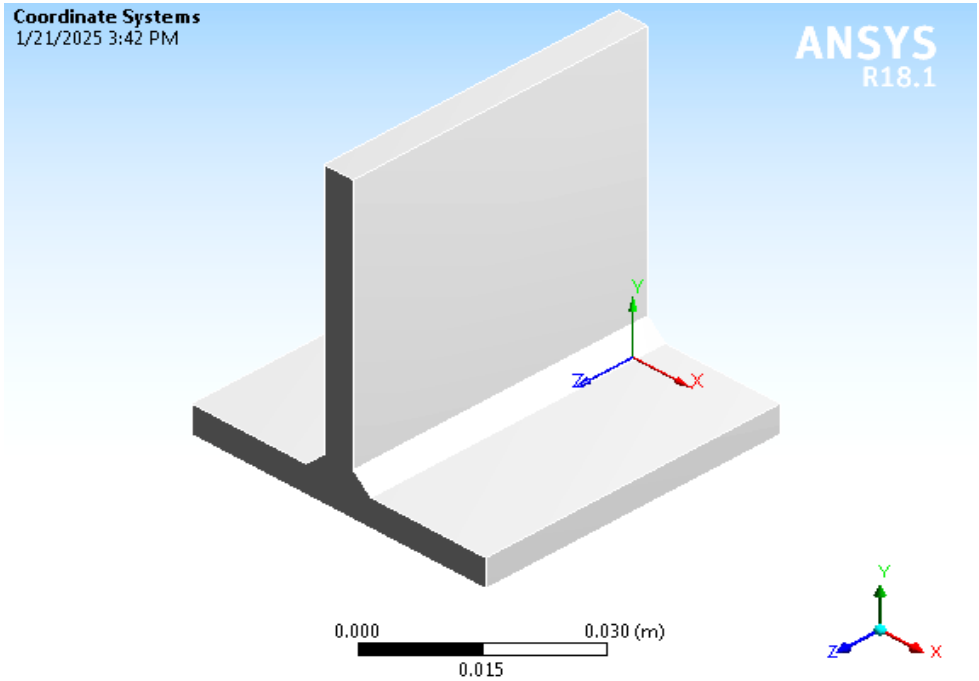

Figure 1. Model of T-section.

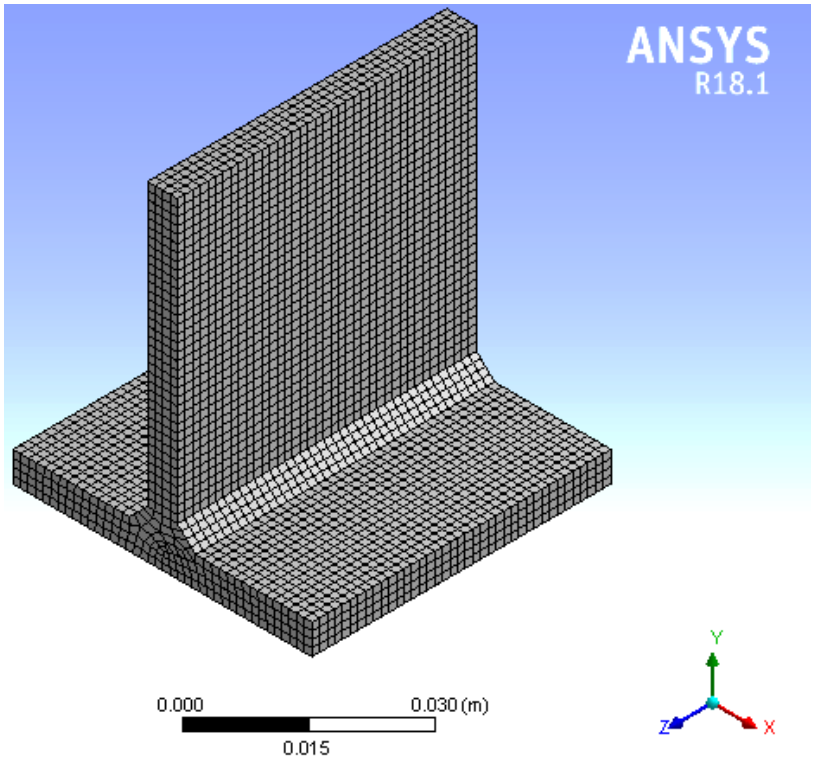

Figure 2. Mesh geometry of T-section.

The present study will be carried out the welding process in the single side as well as double side welding to predict the heat transfer phenomenon. The welding process is carried out in the longitudinal direction (Z-axis). ANSYS is a useful tool used for carrying out the material related study for a heat transfer. In a comparison to the experimental analysis some assumptions take care of the numerical analysis to predict the nonlinear material models. The assumptions are mentioned as

1. Workpiece and tool materials are considered to be homogeneous and isotropic.
2. Work-piece properties are temperature dependent.
3. Heat flux is following the Gaussian distribution principle.
4. The flame is assumed to be axi-symmetric.
5. Fraction of flame is dissipated to work piece.
6. A little amount of weld energy lost to the atmosphere through convection and radiation.
7. Work-piece is considered to be from any stress before machining.

Numerical Methodology

An axisymmetric model with transient analysis of uniform heat flux is considered. In this analysis it is assumed that the work piece is being heated by a Gaussian type of heat source. The heat transfer equation is

$$\frac{1}{\alpha}\frac{\partial T}{\partial t} = \frac{\partial^2 T}{\partial x^2} + \frac{\partial^2 T}{\partial y^2} + \frac{\partial^2 T}{\partial z^2} + Q''' \tag{1}$$

Initial Condition

At t = 0 (initial) welding, the work piece is considered to be at ambient temperature (T_0). Heat generated by the welding in the zone of T-shaped of the joint sp heat flux boundary condition applied in the zone. The other sides of the work pieces are insulated means (dT/dn) = 0, n is the coordinate of the work pieces. Further, the boundary condition of heat flux changed as per the application of the modes of the heat transfer. The heat flux is given in the eq. (2)

$$Q = \frac{4.45 H_i V I}{bL} exp\left\{-4.5\left(\frac{x}{L}\right)^2\right\} \tag{2}$$

The numerical procedure starts with the preparation of the model of the T-joint by defining elements, material and its properties. The mesh is generated and discritize with the help of Finite Element Method (FEM). A grid independence study also carried out independent results of the numerical analysis. The initial and boundary conditions are applied as per the described. The heat flux is applied to solve the problems. The material is considered Maraging steel which is given as per the ANSYS (ANSYS User manual, 2018). The properties selected for the material are density, thermal conductivity, thermal diffusivity, specific heat, Young modulus, Poisson's ratio. The heat transfer data taken into account after a converge solution for further evaluation.

RESULT ANALYSIS

The present numerical work carried out the numerical analysis to determine the heat transfer and the temperature profile through the welding of maraging material process. The numerical analysis was conducted by considering a T-joint. The heat transfer phenomenon predicted the effect of supply current, voltage and diameter of the electrode. The parameter ranges are as current 60 to 90A, voltage 30 to 50V, diameter of electrodes upto 20mm.The data collected from the numerical result is temperature and heat transfer rate calculated.

The Figure 3 shows the contour of the maximum temperature and weld energy during the welding process of T-joint. The Figure 3 shows the maximum temperature occurs in the welding surface. The Figure 4 is illustrating the relationship between maximum temperature and time for different diameters (D) of the welded material. The maximum temperature rises rapidly, reaching its peak of nearly within 2-3 seconds and then gradually declines to 10 second. The Figure 4 shows that as the diameter of the

material increases, the maximum temperature reached over time decreases. This suggests that larger diameters have better heat dissipation, preventing the material from reaching extremely high temperatures quickly. Smaller diameters (0.01 m and 0.012 m) exhibit a rapid increase in temperature and higher peak temperatures compared to larger diameters (0.015 m and 0.02 m). This indicates that smaller diameters have less capacity to dissipate heat, causing them to heat up quickly.

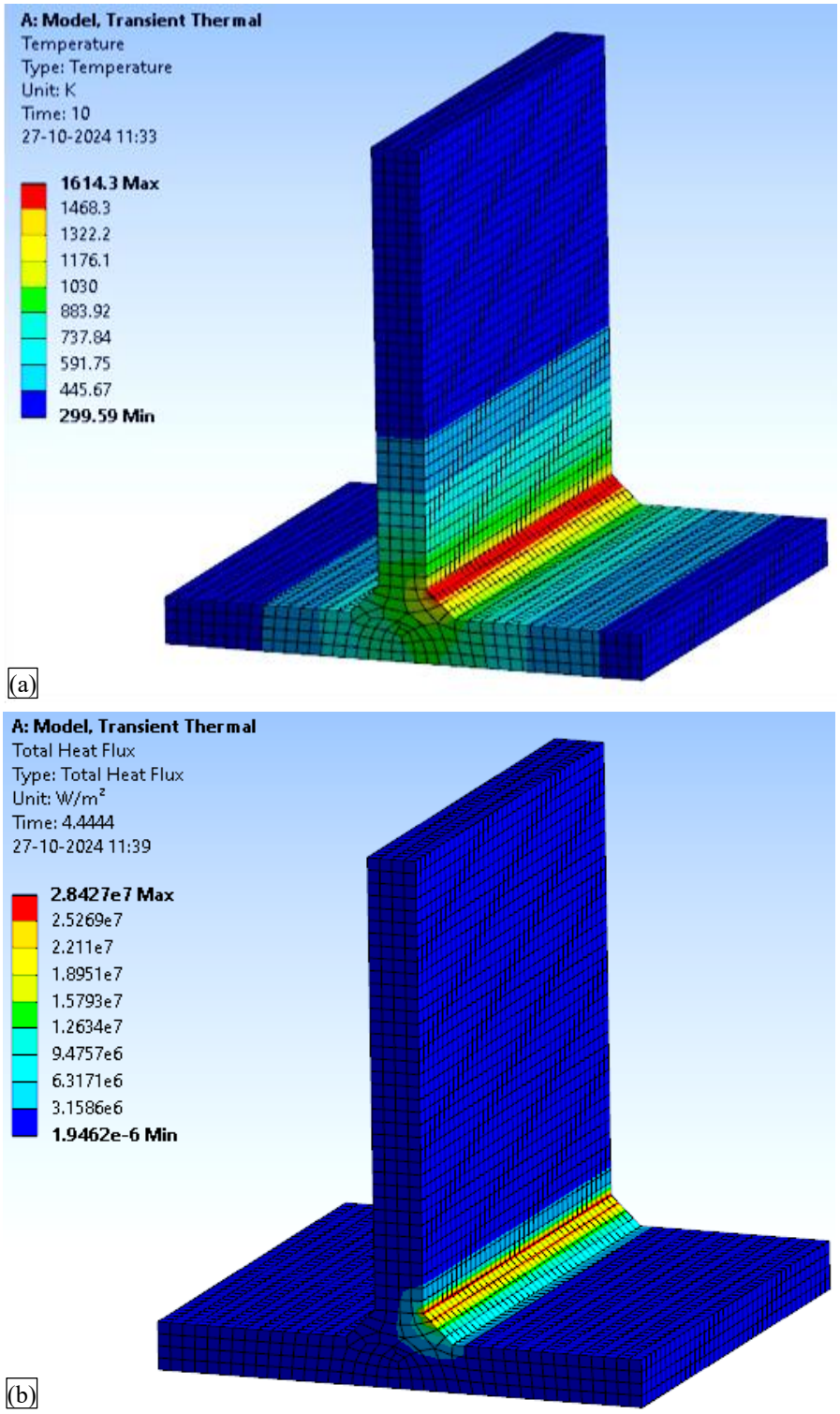

Figure 3. Temperature profile of the T-joint during welding. (a) Maximum Temperature; (b) Weld Energy.

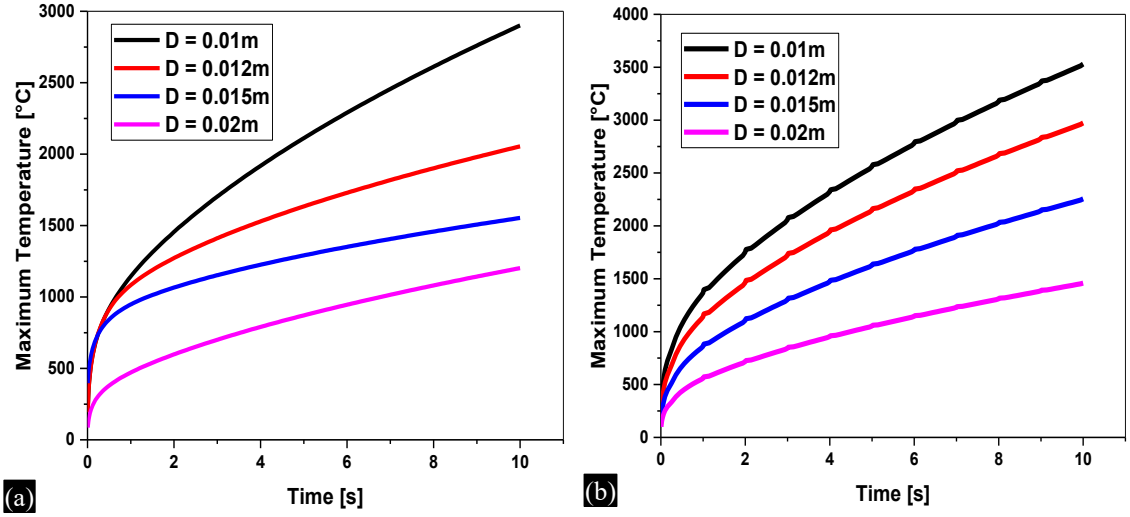

Figure 4. Maximum Temperature of the weld surface for single and double side. (a) Single side; (b) Double side.

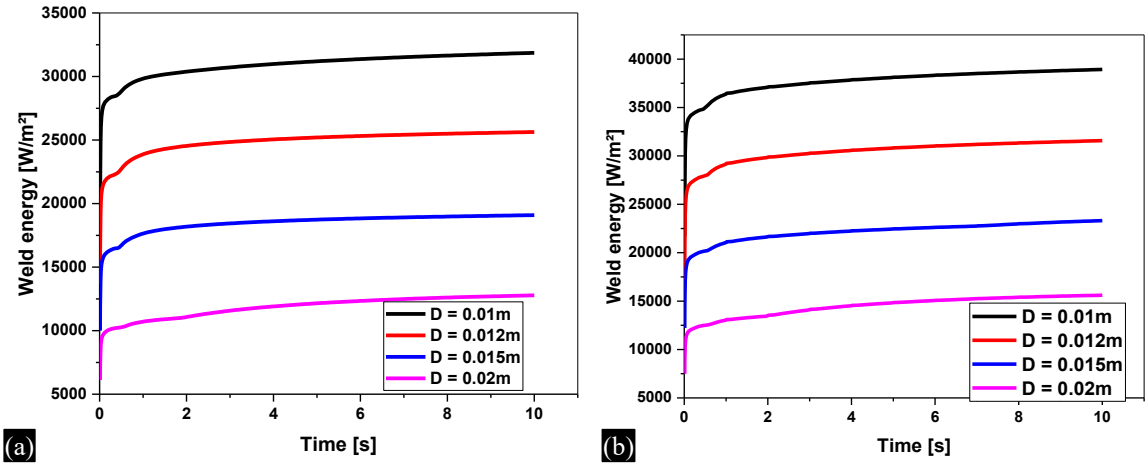

Figure 5. Weld energy of the weld surface for single and double side. (a) Single side; (b) Double side.

This Figure 5 is showing the relationship between weld energy and time for different diameters. As time increases, the weld energy also increases for all diameters, but the rate of increase and the final weld energy values differ for each diameter. The D = 0.01 m reaches the highest weld energy, while the D = 0.02 m reaches the lowest weld energy. Upto 2 seconds, all curves show a rapid increase in weld energy, indicating the initial phase of welding where energy input is high to start the process. Between 2 to 6 seconds, the rate of increase slows down, showing a transition phase where the welding process stabilizes. Finally, from 6 to 10 seconds, the increase becomes more gradual, indicating the latter part of the welding process where the material reaches near its final state. The trend line also finds that smaller diameters reach higher weld energy compared to larger diameters. This suggests that thinner materials require more energy to weld effectively.

Figure 6 depicts the maximum temperature generated on the variation of supply voltage for two different electrode diameters. The trend line suggests that the maximum temperature increases with time. At a particular time the increase in the supply voltage increases the temperature because of more power supplied. The similar trends found in both the electrode diameter on the determination of the maximum temperature. In a comparison between two diameters for a particular supply voltage smaller diameter produces more maximum temperature. The phenomenon occurs because of the large volume of the electrode.

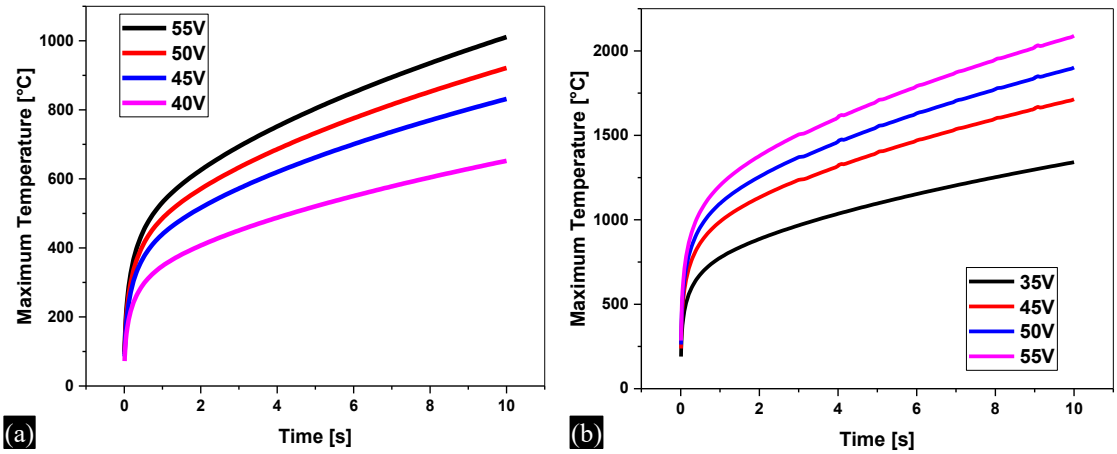

Figure 6. Maximum Temperature of the weld surface for different electrode diameter. (a) Single side, D = 20mm; (b) Single side, D =5mm.

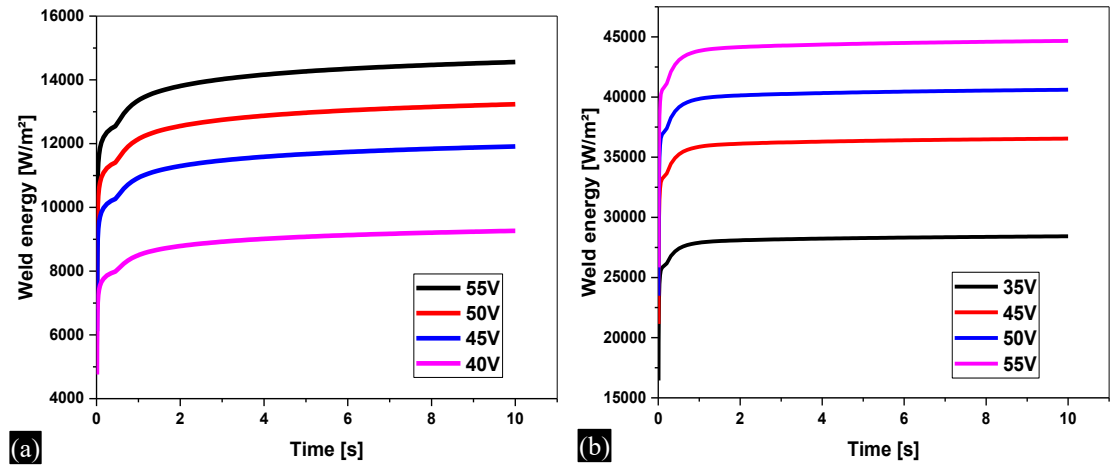

Figure 7. Weld energy of the weld surface for different electrode diameter. (a) Single side, D = 20mm; (b) Single side, D = 5mm.

The Figure 7 depicts weld energy on the variation of supply voltage for two different electrode diameters. The trend line shows the maximum weld energy achieved for the maximum supply voltage and finds the lower electrode diameter produces highest weld energy. The trend line founds this phenomenon because of more heat generated for the welding process on supply of more current.

The Figure 8(a) illustrates the relationship between time and maximum temperature for different input voltages. This steeper ascent indicates that with a higher voltage, the temperature rises more rapidly compared to the lower voltage. The slope of the curve shows an even increase in temperature, demonstrating that a voltage causes a rapid rise in temperature over time. Indicates that at the highest voltage, the maximum temperature increases the fastest and reaches the highest levels. The relationship between weld energy and time for different voltage levels is in the Figure 8(b). As the voltage increases, the weld energy also increases over time. Higher voltage levels result in higher weld energy. As the voltage level increases, the rate at which the weld energy rises also increases. This suggests a direct correlation between voltage and weld energy increase rate. Higher voltage levels result in significantly higher peak weld energies within the same time frame.

Figure 9 depicts the relationship between maximum temperature and time for different modes of heat transfer such as convection and radiation. As the heat transfer coefficient increases, the maximum temperature also increases over time in Figure 9(a). This indicates that materials or systems with higher

heat transfer coefficients absorb more heat in the surrounding air which decrease the temperature and weld energy, but reach higher temperatures with time. Materials with lower heat transfer coefficient experience a sharper increase in temperature, reaching higher maximum temperatures. This indicates that these materials retain heat more effectively but distribute it less efficiently due to surrounding convection effects. Higher heat transfer coefficient release heat more efficiently, resulting in lower maximum temperatures over the same time. The variation of mode of heat transfer for welding predicts the maximum temperatures are shown in Figure 9(b). The trend line suggests the convection and convection- radiation impact on maximum temperature with reducing the maximum temperature.

The Figure 10 depicts the weld energy on the variation of time for modes of heat transfer. The graphs found that the convection and radiation effect on the surrounding of the welding reduces the weld energy generated. The increase in the heat transfer coefficient increases the dissipation of weld energy which reduces the weld energy of the welding. Similarly the combination of convection and radiation also reduces the weld energy from the welding. The mode of the heat transfer in the welding environment improves in the cooling of the work pieces to improve the molecular structure of the welding surfaces.

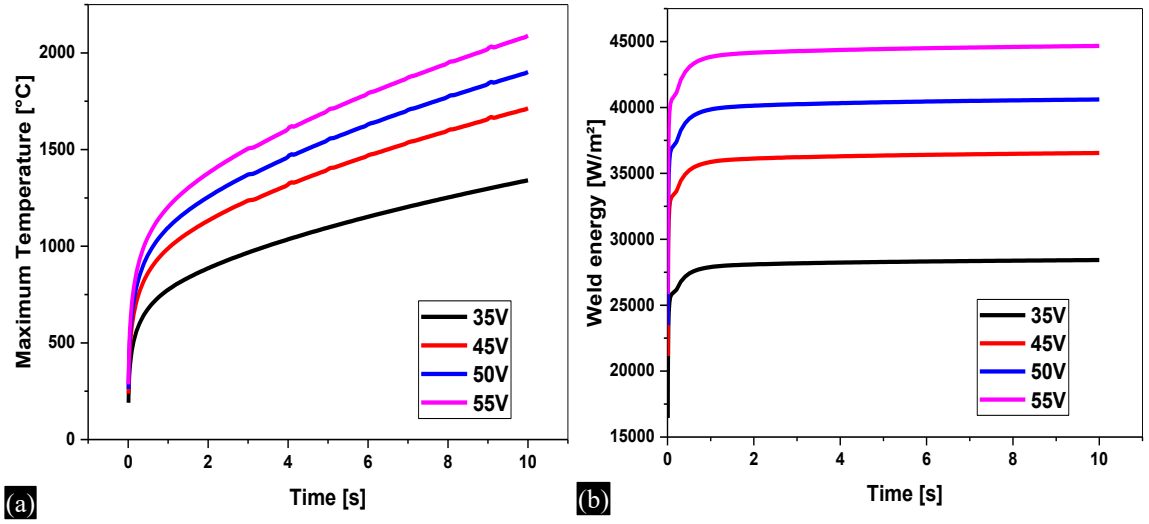

Figure 8. Maximum Temperature of the weld surface for single and double side. (a) Maximum temperature, Single side, D = 5mm; (b) Weld energy, Single side, D =5mm.

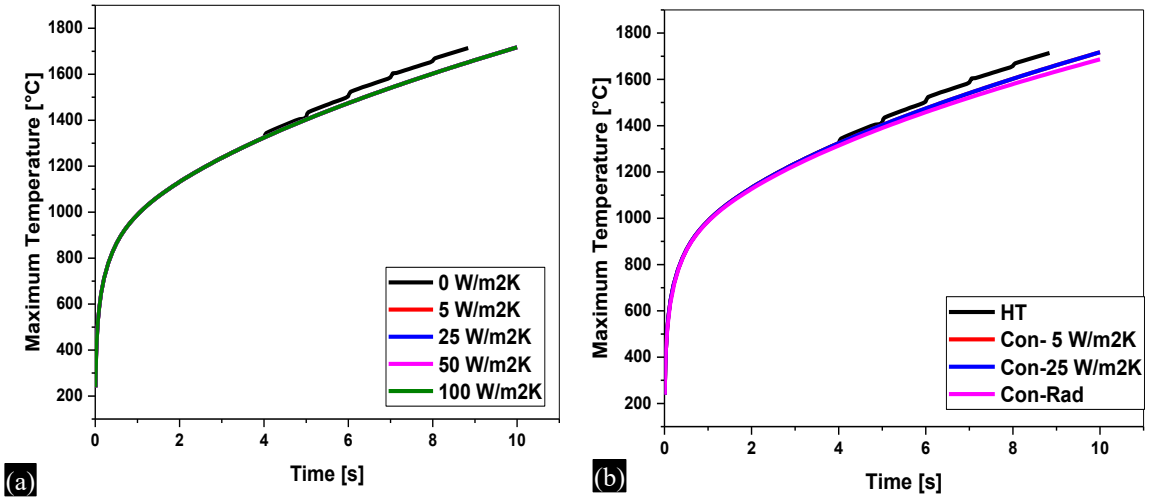

Figure 9. Maximum temperature for different mode of heat transfer. (a) Convection; (b) Convection – Radiation.

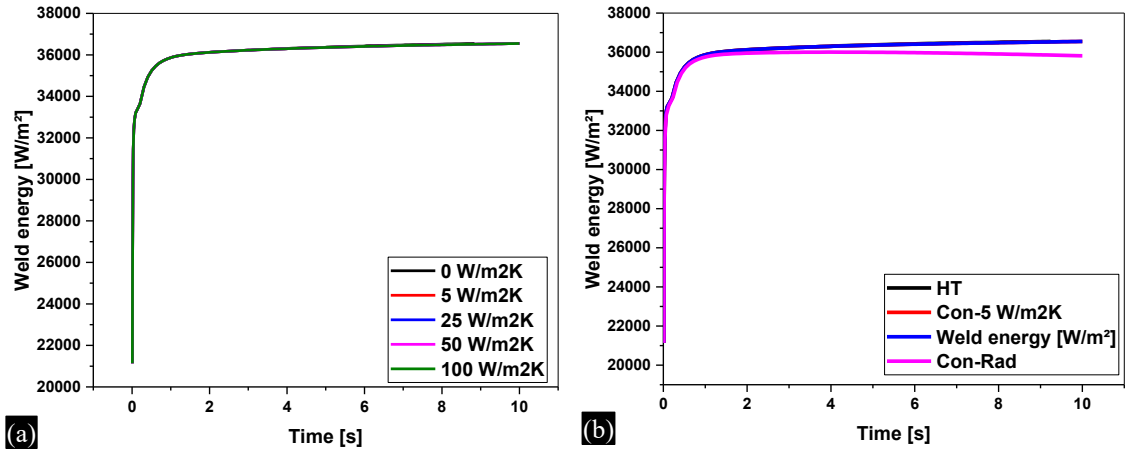

Figure 10. Weld energy for different mode of heat transfer. (a) Convection; (b) Convection – Radiation.

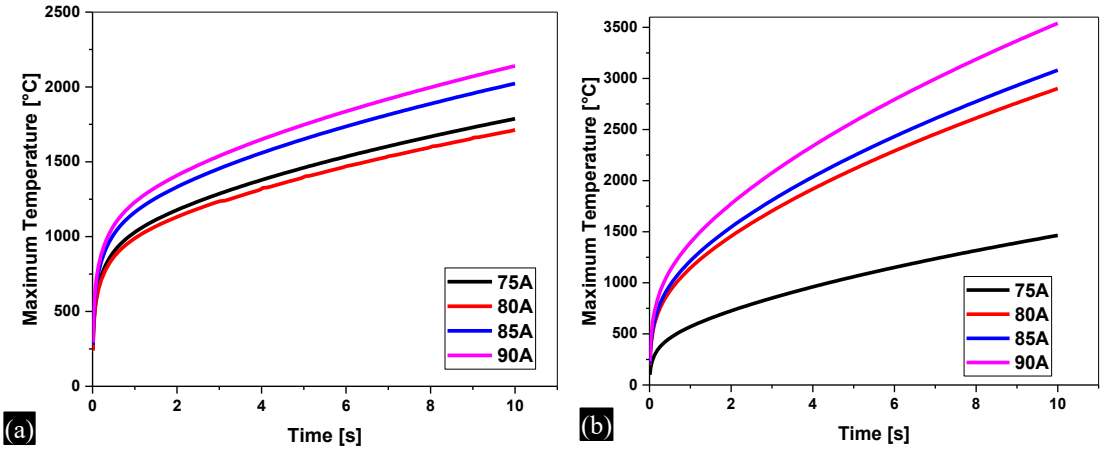

Figure 11. Maximum temperature for single and both sides. (a) Single side; (b) Double side.

Figure 11 showing the relationship between maximum temperature and time for different current values. As the current increases, the maximum temperature also increases over time. Higher current values result in higher maximum temperatures. The rate of temperature increase is higher for higher current values. Higher current levels result in significantly higher peak temperatures within the same time frame. Figure 12 showing the relationship between weld energy and time for different current levels. As the current increases, the weld energy also increases over time. Higher current values result in higher weld energy. Each curve shows that the weld energy tends to level off after a certain period, indicating a steady state in the energy application. Higher currents result in higher weld energies, which can influence the strength and quality of the weld.

CONCLUSION

The present heat transfer analysis of the welding for the maraging steel for different air-craft applications in a numerical study. The study also concludes that the increase in the supply voltage and current increases the supply power which increases the maximum temperature and weld energy generated during the welding process. The electrode diameter also affects the heat transfer phenomenon. The increase in the electrode diameter decreases the heat transfer phenomenon. The mode of the heat transfer such as convection and combined convection-radiation reduces the maximum temperature and weld energy which effect the formation of the welding surface. The study helps to analysis the welding heat transfer of the particular material to improve the design and fabrication of applied components.

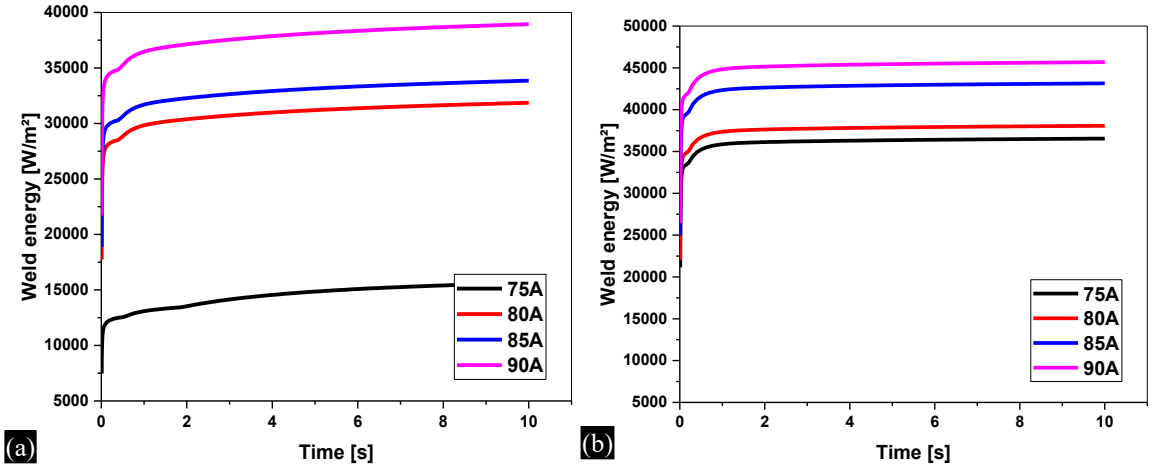

Figure 12. Maximum temperature for single and both sides. (a) Single side; (b) Double side.

Manuscript - with Author Details

Funding

No funding was received by any organization or individual.

Disclosure of Interest

No relevant financial or non-financial competing interests to interest to declare to the publishing from any authors.

Data Availability

The data that support the findings of this study are available on request from the corresponding author, [Santosh Kumar Panda, santumech83@gmail.com]. The data are not publicly available due to [containing information that could compromise the privacy of research participants].

Nomenclature

Symbol	Name
c	Specific heat of the work piece in kJ/kg K
b	Width in m
H	Heat input on work piece W
i	input
I	Current in Ampere
k	Thermal conducvity W/m K
L	Length in m
Q	Heat flux per volume
R	Spark radius in m
V	Voltage in Volt
T	Temperature of the work piece in °C
t	time in sec
x	Axial length variable in m
x, y, z	Coodinate of the system
α	(k/ρc) Thermal diffusivity
ρ	Density of the work piece in kg/m^3

REFERENCES

1. Arora H., Basha K. M., Abhishek. D. B, Devesh B., (2022) Welding simulation of circumferential weld joint using TIG welding process, Vol. 50, Part 5, pp. 923-929. DOI:10.1016/j.matpr.2021.06.315.

2. Arunkumar, M., Dhinakaran, V., & Siva Shanmugam, N. (2019). Numerical prediction of temperature distribution and residual stresses on plasma arc welded thin titanium sheets. International Journal of Modelling and Simulation, 41(2), 146–162. https://doi.org/10.1080/02286203.2019.1700089
3. Aval H. J., Serajzadeh S., and Kokabi A. H., (2010) Theoretical and experimental investigation into friction stir welding of AA 5086," Int. J. Adv. Manuf. Technol. 2010 525, vol. 52, no. 5, pp. 531–544, Jun. 2010, doi: 10.1007/S00170-010-2752-X.
4. Ayoola W.A., Suder W.J., Williams S.W., (2017) Parameters controlling weld bead profile in conduction laser welding, Journal of Materials Processing Technology, Vol. 249, 2017, pp. 522-530, https://doi.org/10.1016/j.jmatprotec.2017.06.026.
5. Baruah M., Bag S., (2017) Influence of pulsation in thermo-mechanical analysis on laser micro-welding of Ti6Al4V alloy, Optics & Laser Technology, Vol. 90, pp. 40-51, https://doi.org/10.1016/j.optlastec.2016.11.006.
6. Campagnolo, A.; Ferro, P.; Romanin, L.; Meneghetti, G. (2021) Residual Notch Stress Intensity Factors in Welded Joints Evaluated by 3D Numerical Simulations of Arc Welding Processes. Materials, 14, 812. https://doi.org/10.3390/ma14040812
7. Chen J, Cao Z, Li J, Guo P., and Sun Y., (2012) Double Wires Submerged Arc Welding Temperature Field Simulation 2nd Int. Conf. on Electronic & Mechanical Engineering and Information Technology (Atlantis Press) 1530–3. doi 10.2991/emeit.2012.339
8. Chludzinski, M, dos Santos, R.E., Churiaque, C., Ortega-Iguña, M., Sánchez-Amaya, J.M., (2021) Pulsed Laser Welding Applied to Metallic Materials—A Material Approach. Metals, 11, 640. https://doi.org/10.3390/met11040640
9. Collins E., E., Joseph I. A., (2017) Analysis of Optimum Butt Welded Joint for Mild Steel Components Using FEM (ANSYS), Advances in Applied Sciences, 2(6): 100-109. doi: 10.11648/j.aas.20170206.12
10. Ebrahimi A., Hermans M. J. M., (2023) Laser butt welding of thin stainless steel 316L sheets in asymmetric configurations: A numerical study, Journal of Advanced Joining Processes, Volume 8, 100154, https://doi.org/10.1016/j.jajp.2023.100154.
11. Farias, R.M., Teixeira, P.R.F., Vilarinho, L.O., (2022) Variable profile heat source models for numerical simulations of arc welding processes, International Journal of Thermal Sciences, Vol. 179, pp. 107593, https://doi.org/10.1016/j.ijthermalsci.2022.107593.
12. Haiying Wei, Yi Zhang, Lipeng Tan, Zhihua Zhong, (2015) Energy efficiency evaluation of hot-wire laser welding based on process characteristic and power consumption, Journal of Cleaner Production, Vol. 87, pp. 255-262, https://doi.org/10.1016/j.jclepro.2014.10.009.
13. He, Kuan Fang, et al., (2011) Three-Dimensional Temperature Field Numerical Simulation of Twin-Arc High-Speed Submerged Arc Welding Process Based on ANSYS." Advanced Materials Research, vol. 216, Trans Tech Publications, Ltd., pp. 188–193. Crossref, doi:10.4028/www.scientific.net/amr.216.188.
14. Hejripour F., Binesh F., Hebel M., Aidun D. K., (2019) Thermal modeling and characterization of wire arc additive manufactured duplex stainless steel, Journal of Materials Processing Technology, Vol. 272, pp. 58-71, https://doi.org/10.1016/j.jmatprotec.2019.05.003.
15. Hossain I., Bhowmik A., Pattanaik A., Kumar, Abhishek R., Singh K. and Pandey S., (2024) Computational investigation of plasma arc welding process for aluminium alloys, Engineering Research Express, Volume 6, Number 2. DOI:10.1088/2631-8695/ad4a24
16. Hua Tan, Yuxun Zhang, Yanxing Liu, Xiaoquan Fu, (2019) ANSYS Workbench simulation of glass welding by femtosecond laser pulses, Infrared Physics & Technology, Volume 98, Pages 334-340, https://doi.org/10.1016/j.infrared.2019.03.036.
17. Jazeel Rahman Chukkan, M. Vasudevan, S. Muthukumaran, R. Ravi Kumar, N. Chandrasekhar, (2015) Simulation of laser butt welding of AISI 316L stainless steel sheet using various heat sources and experimental validation, Journal of Materials Processing Technology, Volume 219, Pages 48-59, https://doi.org/10.1016/j.jmatprotec.2014.12.008.

18. Jain R., Pal S. K., and Singh S. B., (2017) Finite Element Simulation of Temperature and Strain Distribution during Friction Stir Welding of AA2024 Aluminum Alloy, J. Inst. Eng. Ser. C, vol. 98, no. 1, pp. 37–43. doi: 10.1007/s40032-016-0304-3.
19. Kumar, N., Dewangan, R., & Rao, K. R. (2025). Analysis of reinforced friction stir welded joints of dissimilar Al and Cu-alloys by ANSYS software. Welding International, 1–13. https://doi.org/10.1080/09507116.2024.2446254
20. Kurashki S. O, Rogova D. V., Tynchenko Y. A., (2021) Simulation of the electron beam welding process of a bimetallic ring by means of ANSYS, Journal of Physics: Conference Series 2094 (2021) 042092. doi:10.1088/1742-6596/2094/4/042092
21. Lancastr J.F., (1986) The Physics of welding, International Institute of welding, Second Edition. https://doi.org/10.1016/C2013-0-03805-4
22. Lee C. H. and Chang K. H., (2008) Three-dimensional finite element simulation of residual stresses in circumferential welds of steel pipe including pipe diameter effects Materials Science and Engineering: A 487 210–8. DOI:10.1016/j.msea.2007.10.011
23. Liang R., Luo Y., (2017) Study on weld pool behaviors and ripple formation in dissimilar welding under pulsed laser, Optics & Laser Technology, Vol. 93, pp. 1-8, https://doi.org/10.1016/j.optlastec.2017.01.029.
24. Murygin A. V., Kurashkin S. O., Tynchenko V. S. and Rogova D. V., (2021) The use of ANSYS for modelling the energy distribution in steady mode with electron beam welding, Journal of Physics: Conference Series 1889. 042061. doi:10.1088/1742-6596/1889/4/042061
25. Padmanaban R., Ratna K.V., and Balusamy V., "Numerical Simulation of temperature distribution and material flow during friction stir welding of dissimilar aluminum alloys," Procedia Eng., vol. 97, pp. 854–863, Jan. 2014, doi: 10.1016/J.PROENG.2014.12.360.
26. Patterson, T., Hochanadel, J., Sutton, S. et al., (2021) A review of high energy density beam processes for welding and additive manufacturing applications. Weld World 65, 1235–1306. https://doi.org/10.1007/s40194-021-01116-0.
27. Reddy, K.S., Purushotham, A., Kala, K.L. et al., (2024) Thermal mapping of SS316L experimental and simulation for GTA welding process with moving heat source model using FEA. Int J Interact Des Manuf 18, 2755–2763. https://doi.org/10.1007/s12008-023-01310-y
28. Sati P., Shukla D.K., and Tiwari S. K., (2022) Mechanical ANSYS Parametric Design Language Friction Stir Welding Simulation of AZ31B-H24 alloy, IOP Conf. Series: Materials Science and Engineering 1248, 012018. doi:10.1088/1757-899X/1248/1/01201
29. Schnick, M., Fuessel, U., Hertel, M. et al., (2011) Numerical investigations of arc behaviour in gas metal arc welding using ANSYS CFX. Front. Mater. Sci. 5, 98–108 https://doi.org/10.1007/s11706-011-0134-4
30. Semih Taskaya, Ali Kaya Gur, Cetin Ozay, (2019) Joining of Ramor 500 Steel with SAW (Submerged Arc Welding) and its Evaluation of Thermomechanical Analysis in ANSYS Package Software, Thermal Science and Engineering Progress, Vol. 13, 100396, https://doi.org/10.1016/j.tsep.2019.100396.
31. Sonawane H B and Deore E R., (2014) Finite element model for the effect of heat input & speed on residual stress during weldings International Journal of Mechanical Engineering and Robotics Research, vol. 3, pp. 763 ISSN 2278 – 0149 www.ijmerr.com
32. Song M., Kovacevic R., (2003) Thermal modeling of friction stir welding in a moving coordinate system and its validation, Int. J. Mach. Tools Manuf., vol. 43, no. 6, pp. 605–615, May 2003, doi: 10.1016/S0890-6955(03)00022-1.
33. Sattari-Far I and Farahani M R (2009) Effect of the weld groove shape and pass number on residual stresses in butt-welded pipes Int. J. Press. Vessels Pip. Vol. 86, pp. 723–31. https://doi.org/10.1016/j.ijpvp.2009.07.007
34. Tamil Prabakaran, S., Jerome, S., Thirumal, P., Shai Sundaram, V.S., Selvaraju, S., Padmanabhan, S. (2022). Thermal Modelling and Experimental Validation of TIG Welding Using ANSYS. In: Palani, I.A., Sathiya, P., Palanisamy, D. (eds) Recent Advances in Materials and Modern Manufacturing. Lecture Notes in Mechanical Engineering. Springer, Singapore. https://doi.org/10.1007/978-981-19-0244-4_30

35. Tsirkas S. A., Papanikos P., Pericleous K., Strusevich N., Boitout F., Bergheau J. M., (2003) Evaluation of distortions in laser welded shipbuilding parts using local – global finite element approach, Science and Technology of Welding and Joining, Vol. 8 No. 2., https://doi.org/10.1179/136217103225010899
36. Vemanaboina H, Akella S and Buddu R K., (2014) Welding process simulation model for temperature and residual stress analysis Procedia Materials Science, vol. 6, pp. 1539–46. DOI:10.1016/j.mspro.2014.07.135
37. Verma S., Meenu, and Misra J. P., (2017), Study on temperature distribution during Friction Stir Welding of 6082 aluminum alloy, Mater. Today Proc., vol. 4, no. 2, pp. 1350–1356, doi:10.1016/J.MATPR.2017.01.156.
38. Wei, Haiying, Zhang, Yi, Tan, Lipeng, Zhong, Zhihua, (2015), Energy efficiency evaluation of hot-wire laser welding based on process characteristic and power consumption, Journal of Cleaner Production, Vol. 87, pp. 255-262, https://doi.org/10.1016/j.jclepro.2014.10.009.
39. Xu H., Guo X., Lei Y., Lin J., Fu H., Xiao R., Huang T., Shin Y. C., (2019), Welding deformation of ultra-thin 316 stainless steel plate using pulsed laser welding process, Optics & Laser Technology, Vol. 119, pp. 105583, https://doi.org/10.1016/j.optlastec.2019.105583.
40. Zhang Y. M., Yang Y., Zhang W., Na S., (2020) Advanced Welding Manufacturing: A Brief Analysis and Review of Challenges and Solutions, J. Manuf. Sci. Eng., vol. 142(11): pp. 110816. https://doi.org/10.1115/1.4047947

